Calculation of Wannier functions for zinc-blende-type semiconductors

1997 J. Phys.: Condens. Matter 9 5593

(http://iopscience.iop.org/0953-8984/9/26/008)

J. Phys.: Condens. Matter **9** (1997) 5593–5608. Printed in the UK PII: S0953-8984(97)78201-8

Calculation of Wannier functions for zinc-blende-type semiconductors

B Sporkmann and H Bross

Sektion Physik der Ludwig-Maximilians-Universität, Theresienstraße 37, D-80333 München, Germany

Received 30 September 1996, in final form 22 January 1997

Abstract. We calculate generalized symmetrized Wannier functions for the eight-dimensional valence and conduction band complex of zinc-blende-type semiconductors, by Fourier transformation of Bloch functions. A precondition for the success of the procedure is a precise parametrization of the band structure in terms of a Slater–Koster interpolation scheme. The second crucial point is the choice of the phase of the Bloch functions, for which we found a solution even for the case without inversion symmetry. For the materials with diamond structure we obtain s functions whose degree of localization at their respective atomic positions is 60%, and p functions whose degree of localization is 30%. For the materials with zinc-blende structure, the contributions from the four neighbouring atomic spheres have to be added to achieve the same degree of localization. As an application, we use the Wannier functions as a numerical basis when a homogeneous external electric field is applied.

1. Introduction

The construction of localized orbitals from accurate crystal wave functions is closely connected to the Slater–Koster interpolation scheme—or tight-binding (TB) method—where the whole band structure is expressed by means of a small set of parameters, which are matrix elements of localized wave functions. While the TB method is widely applied in semiconductor physics, the corresponding orbitals are not known.

Apart from the general interest in the properties of these functions, there are several possible applications in semiconductor physics. These are for instance in representing localized perturbations such as single atoms or clusters of atoms (quantum dots) or in the improvement of TB calculations for heterostructures by taking into account interface effects and the overlap of the orbitals for different bulk materials. Another possible application is in the study of external fields, where the evaluation of the matrix elements of position or momentum operators is required.

There are two approaches to the calculation of Wannier functions. The direct variational approach proposed by Kohn [1] consists in a minimization of the total energy in terms of Wannier functions. Although very elegant in theory, this method encounters problems in practice, because the periodicity of the crystal potential cannot be exploited. The infinite sums over lattice sites lead to considerable numerical problems, especially in the case of open structures like semiconductors.

These difficulties can be circumvented only by using pseudopotentials, as Tejedor and Vergés [2] did in a calculation for the valence bands of semiconductors, where the resulting pseudo-Wannier functions could be expressed as linear combinations of plane waves.

0953-8984/97/265593+16$19.50

On the other hand, a calculation applying the Fourier transformation to Bloch functions can make use of modern first-principles techniques. However, early attempts in this field [3, 4] were not successful. This is due to two fundamental problems which occur when applying the Fourier transformation to Bloch functions. First, the Bloch functions are not analytical functions of the wave vector $\boldsymbol{k}$ at points of degeneracy. This leads to a breakdown of the convergence of the Fourier series. The second point is that the Bloch functions are determined only up to an arbitrary complex phase factor. The localization of the Wannier functions has to be maximized by an appropriate choice of this phase.

The key to the solution of the first problem lies in the treatment of a band complex, as was shown by Blount, Des Cloizeaux and Bross [5–7]. Teichler [8] has shown that in the case where inversion symmetry holds, the phase is determined up to the sign. On the basis of these considerations, highly localized Wannier functions could be calculated for the fcc transition metals [9]. In the following, these ideas are generalized for a crystal lattice with a basis, and are then applied to semiconductors with diamond and zinc-blende structure.

The paper is organized as follows. We first define generalized Wannier functions in the context of a Slater–Koster interpolation scheme. Special emphasis is put on how the phase of the Bloch functions has to be chosen, even when there is no inversion symmetry. Then we give numerical results concerning the localization properties of the semiconductor Wannier functions.

2. Definition of generalized Wannier functions

2.1. Parametrization of the band structure

We briefly recall the basic ideas of a Slater–Koster interpolation scheme for a crystal lattice with a basis. The one-particle energies and wave functions may be obtained from a first-principles calculation by means of the approximate solution of an effective one-particle Schrödinger equation:

$$\mathcal{H}|n\boldsymbol{k}\rangle = E_{n\boldsymbol{k}}|n\boldsymbol{k}\rangle. \tag{1}$$

$\mathcal{H}$ is the effective one-particle Hamiltonian, $E_{n\boldsymbol{k}}$ the one-particle energy eigenvalue for wave vector $\boldsymbol{k}$ and band n, and $|n\boldsymbol{k}\rangle$ denotes the corresponding Bloch state.

A model Hamiltonian will be constructed which yields the same eigenvalues $E_{n\boldsymbol{k}}$ for a certain number of bands:

$$\mathbf{H}(\boldsymbol{k})\boldsymbol{e}(n,\boldsymbol{k}) = E_{n\boldsymbol{k}}\boldsymbol{e}(n,\boldsymbol{k}) \tag{2}$$

where $\boldsymbol{e}(n,\boldsymbol{k})$ are the eigenvectors. The basis of the crystal lattice may contain N atoms. Then the Hamiltonian matrix consists of $N \times N$ submatrices:

$$\mathbf{H}(\boldsymbol{k}) := \begin{pmatrix} \mathbf{H}^{(11)} & \cdots & \mathbf{H}^{(1N)} \\ \vdots & \ddots & \vdots \\ \mathbf{H}^{(N1)} & \cdots & \mathbf{H}^{(NN)} \end{pmatrix} \tag{3}$$

with the Fourier expansion

$$\mathbf{H}^{(s's)}(\boldsymbol{k}) = \sum_{\boldsymbol{R}} \varepsilon^{(s's)}(\boldsymbol{R}+\boldsymbol{s}'-\boldsymbol{s}) \exp\left[-\mathrm{i}\boldsymbol{k}\cdot(\boldsymbol{R}+\boldsymbol{s}'-\boldsymbol{s})\right]. \tag{4}$$

The superscripts s, s' indicate the submatrices belonging to a pair of basis atoms numbered s and s', respectively, and thus run from 1 to N. The $\boldsymbol{R}$ are the lattice vectors, and the $\boldsymbol{s}$ are the positions of the atoms in the basis with respect to a lattice point. The model Hamiltonian depends on the parameters ε which still have to be determined, but independently of these it should contain all of the symmetries of the problem.

First, we consider the point symmetry. The submatrices of $\mathbf{H}$ transform with the matrices $\mathbf{\Gamma}_s$ for $s = 1, \ldots, N$:

$$\mathbf{H}^{(ss')}(\alpha\boldsymbol{k}) = \mathbf{\Gamma}_s(\alpha)\mathbf{H}^{(ss')}(\boldsymbol{k})\mathbf{\Gamma}_{s'}(\alpha)^{-1} \tag{5}$$

where α denotes an element of the point subgroup, which is defined as the maximum intersection of the point group and the space group. The matrices $\mathbf{\Gamma}_s$ are composed of the representations of the point subgroup which belong to atom s. These representations are determined by the requirement that the eigenvectors $\boldsymbol{e}(n, \boldsymbol{k})$ at symmetric $\boldsymbol{k}$-points transform according to the same representations as the corresponding Bloch functions. Similar symmetry requirements apply for the coefficient matrices:

$$\varepsilon^{(s's)}(\alpha(\boldsymbol{R} + \boldsymbol{s}' - \boldsymbol{s})) = \mathbf{\Gamma}_s(\alpha)\varepsilon^{(s's)}(\boldsymbol{R} + \boldsymbol{s}' - \boldsymbol{s})\mathbf{\Gamma}_{s'}(\alpha)^{-1}. \tag{6}$$

If the Hamilton operator commutes with the inversion operator $\{i, \boldsymbol{t}_i\}$, we have

$$\varepsilon^{(s's)}(\boldsymbol{R} + \boldsymbol{s}' - \boldsymbol{s}) = \varepsilon^{(s'''s'')}(-\boldsymbol{R} - \boldsymbol{s}' + \boldsymbol{s} + \boldsymbol{t}_i) \tag{7}$$

where s''' and s'' are given by $\boldsymbol{s}'' = -\boldsymbol{s} + \boldsymbol{t}_i$ and $\boldsymbol{s}''' = -\boldsymbol{s}' + \boldsymbol{t}_i$, respectively. If spin–orbit coupling is neglected, the $\varepsilon^{(s's)}_{\nu\mu}(\boldsymbol{R} + \boldsymbol{s}' - \boldsymbol{s})$ are real due to time-reversal symmetry [10]. The independent parameters ε which remain after exploiting all of these symmetries have to be determined by means of a non-linear least-squares fit of the model Hamiltonian's eigenvalues (2) to the band-structure energies.

2.2. Definition of the Wannier functions

We now define generalized Wannier functions using the eigenvectors of the model Hamiltonian. These consist of subvectors belonging to the various basis atoms:

$$\boldsymbol{e}(n, \boldsymbol{k}) = (\boldsymbol{e}(n, \boldsymbol{k})^1, \ldots, \boldsymbol{e}(n, \boldsymbol{k})^N) \tag{8}$$

and obey the orthogonality relations

$$\sum_n \boldsymbol{e}(n, \boldsymbol{k})^{s'*}_{\nu} \boldsymbol{e}(n, \boldsymbol{k})^s_{\mu} = \delta_{ss'}\delta_{\nu\mu} \tag{9}$$

$$\sum_{s\nu} \boldsymbol{e}(n', \boldsymbol{k})^{s*}_{\nu} \boldsymbol{e}(n, \boldsymbol{k})^s_{\nu} = \delta_{nn'}. \tag{10}$$

Because of (5), they transform with the matrices $\mathbf{\Gamma}_s$:

$$\boldsymbol{e}(n, \alpha\boldsymbol{k})^s = \mathbf{\Gamma}_s(\alpha)\boldsymbol{e}(n, \boldsymbol{k})^s. \tag{11}$$

A Wannier function of symmetry ν centred at $\boldsymbol{R} + \boldsymbol{s}$ is defined by the following unitary transformation:

$$|\nu\boldsymbol{s}\boldsymbol{R}\rangle \equiv \frac{\Omega^{1/2}}{(2\pi)^{3/2}} \int_{\mathcal{BZ}} \mathrm{d}\boldsymbol{k}\ \exp[-\mathrm{i}\boldsymbol{k}\cdot(\boldsymbol{s} + \boldsymbol{R})] \sum_n \boldsymbol{e}(n, \boldsymbol{k})^{s*}_{\nu} |n\boldsymbol{k}\rangle \tag{12}$$

where Ω is the volume of the Wigner–Seitz cell and $\mathcal{BZ}$ the first Brillouin zone.

The reciprocal relation is

$$|n\boldsymbol{k}\rangle = \frac{\Omega^{1/2}}{(2\pi)^{3/2}} \sum_s \sum_{\boldsymbol{R}} \exp[\mathrm{i}\boldsymbol{k}\cdot(\boldsymbol{s} + \boldsymbol{R})] \sum_{\nu} \boldsymbol{e}(n, \boldsymbol{k})^s_{\nu} |\nu\boldsymbol{s}\boldsymbol{R}\rangle. \tag{13}$$

Then the coefficients in (4) are the energy matrix elements of the Wannier functions:

$$\varepsilon^{(s's)}_{\mu\nu}(\boldsymbol{R}' - \boldsymbol{R} + \boldsymbol{s}' - \boldsymbol{s}) = \langle \mu\boldsymbol{s}'\boldsymbol{R}'|\boldsymbol{H}|\nu\boldsymbol{s}\boldsymbol{R}\rangle. \tag{14}$$

In the following, these are called Slater–Koster (SK) parameters. From the orthogonality of the Bloch functions and the eigenvectors (9), one obtains the orthogonality relations for the Wannier functions:

$$\langle \mu s' \boldsymbol{R}' | \nu s \boldsymbol{R} \rangle = \delta_{ss'} \delta_{\nu\mu} \delta_{\boldsymbol{R}\boldsymbol{R}'}. \tag{15}$$

Application of a space group operation $\{\alpha, \boldsymbol{a}\}$ yields

$$\{\alpha, \boldsymbol{a}\} | \nu s \boldsymbol{R} \rangle = \sum_{\mu} \Gamma_s(\alpha^{-1})_{\nu\mu} | \mu, \alpha s, \alpha \boldsymbol{R} + \boldsymbol{a} \rangle. \tag{16}$$

Thus, the Wannier functions transform like basis functions to the irreducible representations of the point subgroup. In the appendix it is shown that this transformation property requires the following condition for degenerate states n and n' at symmetric $\boldsymbol{k}$-points:

$$\sum_{s} \sum_{\mu\nu} \Gamma_s(\beta)^{-1}_{\nu\mu} \boldsymbol{e}(n, \boldsymbol{k})^{s\,*}_{\mu} \boldsymbol{e}(n', \boldsymbol{k})^{s}_{\nu} = \langle n' \boldsymbol{k} | \{\beta, \boldsymbol{t}_\beta\} | n \boldsymbol{k} \rangle \tag{17}$$

for an element $\{\beta, \boldsymbol{t}_\beta\}$ of the little group of $\boldsymbol{k}$. This corresponds to the degenerate eigenvectors in their subspace adopting the orientation of the corresponding degenerate Bloch functions.

With spin–orbit coupling neglected, time-reversal symmetry yields, up to a phase factor,

$$\langle \boldsymbol{r} | n, -\boldsymbol{k} \rangle = \langle n \boldsymbol{k} | \boldsymbol{r} \rangle \tag{18}$$

$$\boldsymbol{e}(n, -\boldsymbol{k})^{s} = \boldsymbol{e}(n, \boldsymbol{k})^{s\,*}. \tag{19}$$

If this phase factor is chosen equal in the two cases, it cancels in (12). As always, both $\boldsymbol{k}$ and $-\boldsymbol{k}$ appear in the integration over the Brillouin zone, the Wannier functions are real:

$$\langle \boldsymbol{r} | \nu s \boldsymbol{R} \rangle = \int_{\mathcal{BZ}} \sum_{n} \mathrm{Re} \left\{ \boldsymbol{e}(n, \boldsymbol{k})^{s\,*}_{\nu} \langle \boldsymbol{r} | n \boldsymbol{k} \rangle \exp\left[-\mathrm{i} \boldsymbol{k} \cdot \boldsymbol{s}\right] \right\} \, \mathrm{d}\boldsymbol{k}. \tag{20}$$

In some cases it might be useful to perform the Fourier transformation only in one direction perpendicular to a given crystal plane, or equivalently to combine the Wannier functions of this plane. Let $\boldsymbol{a}_1$ and $\boldsymbol{a}_2$ be the in-plane basis vectors of the lattice, $\boldsymbol{a}_3$ the third one, and $\boldsymbol{R} = l_1 \boldsymbol{a}_1 + l_2 \boldsymbol{a}_2 + l \boldsymbol{a}_3$. Then we can define layer Wannier functions for a fixed wave vector $\boldsymbol{k}_\perp$ perpendicular to $\boldsymbol{a}_3$:

$$| \boldsymbol{k}_\perp, \nu s l \rangle = \sum_{l_1, l_2} \exp\left[\boldsymbol{k}_\perp \cdot (l_1 \boldsymbol{a}_1 + l_2 \boldsymbol{a}_2)\right] | \nu s \boldsymbol{R} \rangle. \tag{21}$$

It is to be emphasized that the model Hamiltonian and the Wannier functions crucially depend on the choice of the independent Slater–Koster parameters. From equation (14) it follows directly that localized Wannier functions can be expected only if the Fourier expansion (4) converges quickly.

2.3. Choice of the phase

Apart from the degeneracies, the second fundamental problem in the construction of Wannier functions from Bloch functions is the choice of the phase of the latter. Here, two cases have to be distinguished.

2.3.1. Inversion symmetry. In the case of inversion symmetry, there is either only one atom in the basis—this simpler case was considered in reference [9]—or there are always two identical atoms at positions $\boldsymbol{s}_1$ and $\boldsymbol{s}_2$, with

$$\boldsymbol{s}_1 = \{i, \boldsymbol{t}_i\}\boldsymbol{s}_2 \tag{22}$$

where $\{i, \boldsymbol{t}_i\}$ denotes the inversion operator. Then the phase of the eigenvectors $\boldsymbol{e}(n, \boldsymbol{k})$ can be chosen such that the subvectors belonging to these two identical atoms are complex conjugates of each other:

$$\boldsymbol{e}(n, \boldsymbol{k})^2 = \boldsymbol{e}(n, \boldsymbol{k})^{1^*}. \tag{23}$$

This corresponds to a real formulation of the Slater–Koster interpolation scheme. Similarly, a real formulation of the first-principles scheme yields

$$\langle \boldsymbol{r}|\{i, \boldsymbol{t}_i\}|n\boldsymbol{k}\rangle = \langle n\boldsymbol{k}|\boldsymbol{r}\rangle. \tag{24}$$

Teichler [8] has shown that this choice leads to a maximum localization of the common bond and anti-bond orbitals, $|\nu, +, \boldsymbol{R}\rangle$ and $|\nu, -, \boldsymbol{R}\rangle$, in the sense that the expectation value of r^2 takes on its minimum value. They are related to our atom-centred Wannier functions via

$$|\nu, \pm, \boldsymbol{R}\rangle = \frac{1}{\sqrt{2}}(|\nu\boldsymbol{s}_1\boldsymbol{R}\rangle \pm |\nu\boldsymbol{s}_2\boldsymbol{R}\rangle). \tag{25}$$

The maximum localization of the bond orbitals is equivalent to that of the Wannier functions at sites $\boldsymbol{s}_1$ and $\boldsymbol{s}_2$. From equations (12), (23), and (24), it follows also that

$$\langle \boldsymbol{r}|\{i, \boldsymbol{t}_i\}|\nu\boldsymbol{s}_1, -\boldsymbol{R}\rangle = \langle \boldsymbol{r}|\nu\boldsymbol{s}_2\boldsymbol{R}\rangle. \tag{26}$$

This means that we have identical Wannier functions at sites $\boldsymbol{s}_1$ and $\boldsymbol{s}_2$ if we have identical atoms at the two positions. Thus the introduction of a complex phase would result in an artificial asymmetry.

There still remains the choice between $+1$ and -1 for the phase. This has to be made in such a manner that abrupt changes of sign are avoided, and smooth functions in $\boldsymbol{k}$-space are obtained under the integral in equation (12).

2.3.2. No inversion symmetry. In the case without inversion symmetry, the problem cannot be formulated in terms of real-valued entities. Thus the problem of the choice of the phase cannot be reduced to the alternatives ± 1. Nevertheless, a solution can be found in analogy to the symmetric case. The wave functions, as well as the SK eigenvectors, are decomposed into a part exhibiting inversion symmetry and a rest term:

$$|n\boldsymbol{k}\rangle = |n\boldsymbol{k}\rangle^I + |n\boldsymbol{k}\rangle^R \tag{27}$$

$$\boldsymbol{e}(n, \boldsymbol{k})^s = \boldsymbol{e}(n, \boldsymbol{k})^{s\,I} + \boldsymbol{e}(n, \boldsymbol{k})^{s\,R} \qquad s = 1, 2 \tag{28}$$

with

$$\langle \boldsymbol{r}|n\boldsymbol{k}\rangle^I = \frac{1}{2}(\langle \boldsymbol{r}|n\boldsymbol{k}\rangle + \langle n\boldsymbol{k}|\{i, \boldsymbol{t}_i\}|\boldsymbol{r}\rangle) \tag{29}$$

$$\boldsymbol{e}(n, \boldsymbol{k})^{1^I} = \frac{1}{2}(\boldsymbol{e}(n, \boldsymbol{k})^1 + \boldsymbol{e}(n, \boldsymbol{k})^{2^*}) \tag{30}$$

$$\boldsymbol{e}(n, \boldsymbol{k})^{2^I} = \boldsymbol{e}(n, \boldsymbol{k})^{1^{I^*}}. \tag{31}$$

However, this decomposition is not yet unique, because both the wave function and the SK eigenvector can be multiplied by an arbitrary complex phase:

$$|\widetilde{n\boldsymbol{k}}\rangle = |n\boldsymbol{k}\rangle \mathrm{e}^{\mathrm{i}\chi} \tag{32}$$

$$\tilde{\boldsymbol{e}}(n, \boldsymbol{k})_\nu^{1,2} = \boldsymbol{e}(n, \boldsymbol{k})_\nu^{1,2} \mathrm{e}^{\mathrm{i}\xi}. \tag{33}$$

The contributions to the norm resulting from the symmetrized parts as functions of ξ and χ are

$$|\tilde{e}(n,\boldsymbol{k})^I|^2(\xi) = \frac{1}{2} + \frac{1}{2}\mathrm{Re}\left(\mathrm{e}^{2\mathrm{i}\xi}\sum_\nu \boldsymbol{e}(n,\boldsymbol{k})^1_\nu \boldsymbol{e}(n,\boldsymbol{k})^2_\nu\right) \tag{34}$$

$$\langle\widetilde{n\boldsymbol{k}}|^I\widetilde{n\boldsymbol{k}}\rangle^I(\chi) = \frac{1}{2} + \frac{1}{2}\mathrm{Re}(\mathrm{e}^{-2\mathrm{i}\chi}\langle n\boldsymbol{k}|\{i,\boldsymbol{t}_i\}|n\boldsymbol{k}\rangle). \tag{35}$$

For each n and each $\boldsymbol{k}$, χ and ξ are chosen such that they maximize these expressions. The relative phase is then set to ± 1 taking into account only the symmetric parts, in analogy to the case with inversion symmetry.

The idea of this procedure is simply to disregard the asymmetric contributions, and to treat, for example, a III–V compound like an element of the fourth group as far as the choice of the phase is concerned.

An alternative method is to choose the phase such that the expression

$$\exp[-\mathrm{i}\boldsymbol{k}\cdot\boldsymbol{s}]\boldsymbol{e}(n,\boldsymbol{k})^{s\,*}_\nu\langle\boldsymbol{r}|n\boldsymbol{k}\rangle$$

is real and positive at the centre of the Wannier function $|\nu\boldsymbol{s}\boldsymbol{0}\rangle$ or close to the centre in the case in which the Wannier function vanishes there for symmetry reasons. Here, the idea is that the localization in the central sphere is maximized, because according to equation (20) the imaginary part does not contribute.

In general the first method is to be preferred because of its symmetric character, in contrast to the second one, which selects one particular atom s.

3. Results

We considered the semiconductors of the fourth group of the periodic table which crystallize in the diamond structure, and several III–V compounds with zinc-blende structure. The Bloch functions were taken from the MAPW calculations of Bross and Bader [11, 12], which were carried out within the non-relativistic local density approximation (LDA) using the density functional according to Gunnarsson and Lundquist [13]. The most important features of the wave functions obtained from the MAPW procedure are that they are orthogonal to the core states and everywhere differentiable in $\boldsymbol{r}$, so the Wannier functions will have the same properties. In a more rigorous treatment, the heavier materials should be treated in a relativistic frame, but for our considerations a non-relativistic treatment is sufficient. It is a well known shortcoming of such calculations that the band gap obtained is too small compared to experimental data, but the ground-state properties can be described satisfactorily. Details about the numerical representation of the Bloch functions used to construct the Wannier functions can be found, for example, in [12].

The zinc-blende structure consists of an fcc lattice with a basis of two atoms, which in general are not identical. The diamond structure constitutes the special case in which they are identical. The point subgroup is the tetrahedral group $\mathrm{T_d}$ of order 24, which is also the point group in the case of the zinc-blende structure. The point group of the diamond structure is the cubic group $\mathrm{O_h}$ of order 48, due to the additional inversion symmetry.

3.1. Parametrization of the band structure

We employed the usual eight-band model Hamiltonian consisting of one s function and three p functions per atom. So the band complex considered consists of the four valence bands and the first four conduction bands. It is defined by the point group representations

at $\boldsymbol{k} = 0$. These are, with increasing energy, Γ_1, Γ_{15}, Γ_1, and Γ_{15} of T_d for the zinc-blende structure, and Γ_1, $\Gamma_{25'}$, $\Gamma_{2'}$, and Γ_{15} of O_h for the diamond structure, respectively. The splitting into even and odd representations for the valence and the conduction bands in the case of the diamond structure is due to the additional inversion symmetry. But the subduced representations of the point subgroup T_d are the same as for the zinc-blende structure. So we have for both atoms

$$\boldsymbol{\Gamma}_s(\alpha) = \begin{pmatrix} \boldsymbol{\Gamma}^1(\alpha) & 0 \\ 0 & \boldsymbol{\Gamma}^{15}(\alpha) \end{pmatrix} \qquad s = 1, 2. \tag{36}$$

In the following, the Wannier functions will also be called s functions (Γ^1) and p functions (Γ^{15}: x, y, z). Note that they do not exhibit definite parity, in contrast to their atomic counterparts.

In agreement with Papaconstantopoulos [14], we find for all materials that the MAPW wave function of the fifth conduction band at the point W does not contain s symmetry, but contains d symmetry, while it is s-like at the point X. This strong mixing of s and d symmetries would imply an enlargement of the sp model by both types of symmetry. So in contrast to the empirical tight-binding method, the sps* model [15] is not suitable for our aims, since we try to adapt the SK model Hamiltonian to the first-principles band structure as precisely as possible. However, due to the high-dimensional and non-linear nature of this problem, the enlargement is difficult to perform.

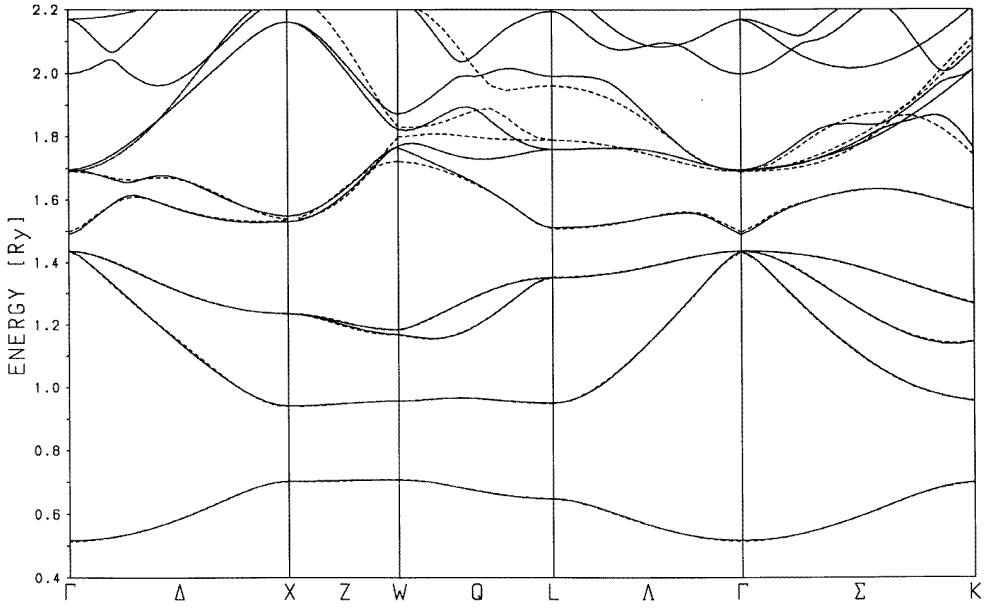

Figure 1. The band structure of GaAs. ——: MAPW; - - - -: interpolation.

The fit of the independent SK parameters (14) was carried out at 110 $\boldsymbol{k}$-points in the irreducible wedge of the Brillouin zone. We considered interactions up to the fourth neighbours. The result is a precise reproduction of the valence bands in the range of accuracy of the first-principles calculations and of the first two conduction bands on a mRyd scale. The mean errors of the interpolation are given in tables 1 and 2. Figure 1 shows the parametrized band structure of GaAs compared to the first-principles band structure.

Table 1. Mean errors of the Slater–Koster interpolation for the diamond structure, in mRyd.

Band	C	Si	Ge	α-Sn
Valence	2.0	1.7	1.4	1.4
Fifth	6.2	7.1	9.7	4.2
Sixth	55.5	40.1	34.5	22.5

Table 2. Mean errors of the Slater–Koster interpolation for the zinc-blende structures, in mRyd.

Band	BN	AlP	GaAs	AlAs	InSb	GaP	InP	SiC
Valence	1.7	1.8	1.7	1.8	0.5	1.0	0.5	1.1
Fifth	4.7	8.7	3.1	2.9	3.3	2.7	4.6	8.7
Sixth	43.0	29.4	24.9	31.3	16.1	26.7	10.0	43.6

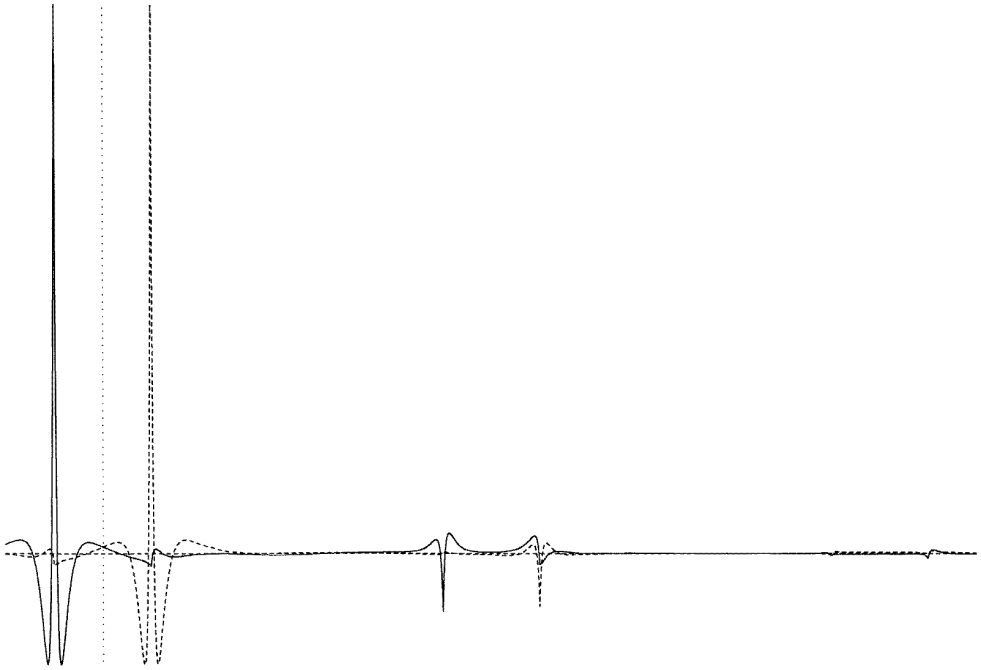

Figure 2. Wannier functions with s symmetry for Si in the (111) direction. The Wannier functions are centred at the atoms next to the dotted mirror axis. The precise positions of the nuclei coincide with the most distinctive local maxima of the functions, which are due to the s-like parts present in all spheres.

As can be seen from the band structure, the deviations for the conduction bands are large in the neighbourhoods of the points W, L, and K, while the agreement is much better in the interior of the Brillouin zone and in particular at the conduction band edge. If, for example, for GaAs only the deviations below the conduction energy Γ^{15} (at 1.7 Ryd in figure 1) are considered, there remains a mean error of only 2.3 mRyd for the conduction bands in this region. The SK parameters will not be given here, since they depend sensitively on the

approximations made in the calculation of the band structure†. In general, it is important to use a first-principles scheme which yields well converged wave functions in order to guarantee that the band structure does not show artificial steps in $\boldsymbol{k}$-space, which would prevent a precise fit.

3.2. Phase

It was stated in section 2.3 that in both cases, the diamond structure and the 'symmetrized' zinc-blende structure related to it, we still have to determine the appropriate sign of the integrand in equation (12). While the two atoms are coupled by the reality condition (23), there is no prescription for the weights of the different components ν of the subeigenvector $\boldsymbol{e}(n,\boldsymbol{k})^s$. It turns out that the highest degree of localization for all symmetries is obtained when only the s symmetry is taken into account here, instead of, for example, the symmetry with the largest amplitude for a particular $(n,\boldsymbol{k})$. This can be understood *a posteriori* by considering the higher degree of localization of the s functions. Thus, we simply require

$$\mathrm{Re}(\exp[-\mathrm{i}\boldsymbol{k}\cdot\boldsymbol{s}]\boldsymbol{e}(n,\boldsymbol{k})_\nu^{s\,*}\langle\boldsymbol{r}=\boldsymbol{0}|n\boldsymbol{k}\rangle) > 0 \tag{37}$$

for all $(n,\boldsymbol{k})$.

The symmetrizing procedure works in all cases except those of BN and SiC, where the other method was used. The failure in these cases is due to the lack of 'diamond-like' symmetry in the electronic charge density of these materials (see, e.g., for BN, reference [12]). In all other cases the second method has also been applied in order to check the results of the symmetrizing method. As no qualitative differences appeared, it can be said that the results for the localization of the Wannier functions given below are reasonable.

3.3. Localization

As a measure for the localization of the Wannier functions, the norm integral confined to the central muffin-tin sphere is used:

$$P_\nu^s \equiv \int_{MTS} |\langle\boldsymbol{r}|\nu\boldsymbol{s}\boldsymbol{0}\rangle|^2 \;\mathrm{d}\boldsymbol{r}. \tag{38}$$

The values are given in table 3.

Table 3. The norm integral P_ν in the central muffin-tin sphere of Wannier functions for diamond structure.

	s	p
C	0.59	0.53
Si	0.60	0.28
Ge	0.66	0.32
Sn	0.65	0.34

For the diamond structure, we find an average localization of 60% in the central sphere for the s function and 30% for the p function. So the s functions are much more fully localized than the p functions. An exception is diamond itself, where the value for the p function is almost as large as the one for the s function. No significant localization can be found in the remaining spheres. This means that the rest of the norm is smeared out over

† The parameters are available from the authors on request.

Table 4. The norm integral P_ν in the central and adjacent muffin-tin spheres of Wannier functions for zinc-blende structure.

	III component				V component			
	s		p		s		p	
	Central	Adjacent	Central	Adjacent	Central	Adjacent	Central	Adjacent
BN	0.32	0.01	0.14	0.01	0.18	0.05	0.13	0.06
AlP	0.31	0.02	0.17	0.01	0.22	0.04	0.14	0.06
GaAs	0.28	0.04	0.16	0.01	0.21	0.06	0.17	0.05
AlAs	0.26	0.03	0.15	0.01	0.16	0.06	0.13	0.05
InSb	0.32	0.04	0.17	0.005	0.25	0.06	0.15	0.04
GaP	0.33	0.03	0.21	0.004	0.29	0.04	0.15	0.05
InP	0.32	0.03	0.19	0.005	0.21	0.05	0.11	0.06
	Si				C			
SiC	0.34	0.01	0.19	0.01	0.22	0.04	0.13	0.05

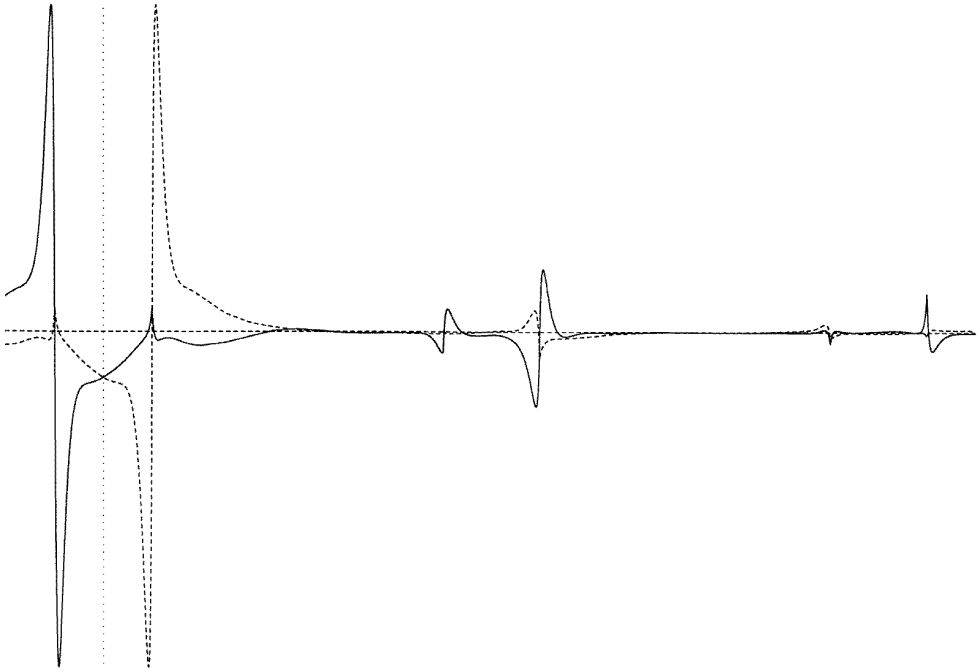

Figure 3. Wannier functions with p symmetry for Si in the (111) direction. The Wannier functions are centred at the atoms next to the dotted mirror axis. The precise positions of the nuclei coincide with the most distinctive local maxima of the functions, which are due to the s-like parts present in all spheres.

the whole space. For silicon, the behaviour of the functions is illustrated in figures 2 and 3. In agreement with the values in table 3, the s functions fall off much more quickly than the p functions. In the case of the III–V compounds as well, the s functions are better localized than the p functions. However, here all of the functions are less localized in the central sphere than in the case of the diamond structure. Considerable contributions are found

also in the four adjacent atomic spheres. On adding these, the same order of magnitude is obtained for the degree of localization. Note that there exists an asymmetry of the two components. The group III Wannier functions are much more fully localized in the central sphere than the group V functions, especially the s functions. On the other hand, the group V functions, in particular the p functions, make larger contributions in the four adjacent spheres, so their degree of localization in all of the five spheres taken together exceeds that of the group III functions. This is in agreement with reference [12], where it is shown for BN that, due to the charge shift from the boron to the nitrogen atom, the size of the latter is increased, in the sense that the spherical form of the charge density around the N nucleus extends into the adjacent spheres, while that around the B nucleus is contained in the interior of its own muffin-tin sphere. The values for the localization are given in table 4.

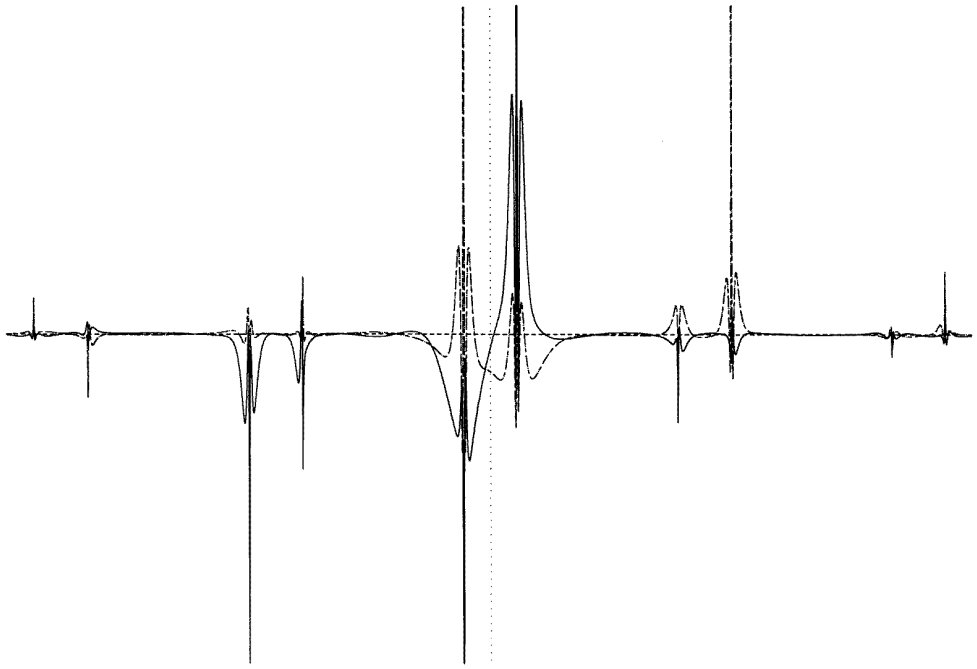

Figure 4. Wannier functions with s symmetry for GaAs in the (111) direction. ——: Ga; - - - -: As. The Ga function is centred at the atom to the left of the dotted mirror axis, and the As function at that to the right. The precise positions of the nuclei coincide with the most distinctive local maxima of the functions, which are due to the s-like parts present in all spheres.

As examples, the Wannier functions for GaAs are shown in figures 4 and 5. The number of nodes in the central sphere is determined by the symmetry type and the row in the periodic table, in analogy to atomic 4s or 4p functions. The two components show a tendency towards symmetry with respect to the mirror axis, in agreement with the choice of phase applied.

While the degree of localization and the shape of the Wannier functions in the central sphere are not sensitive to the mesh used for the integration in (12), the shape of the Wannier functions far away from the centre of course is. So the integration mesh has to be refined until the precision required by a certain application is achieved.

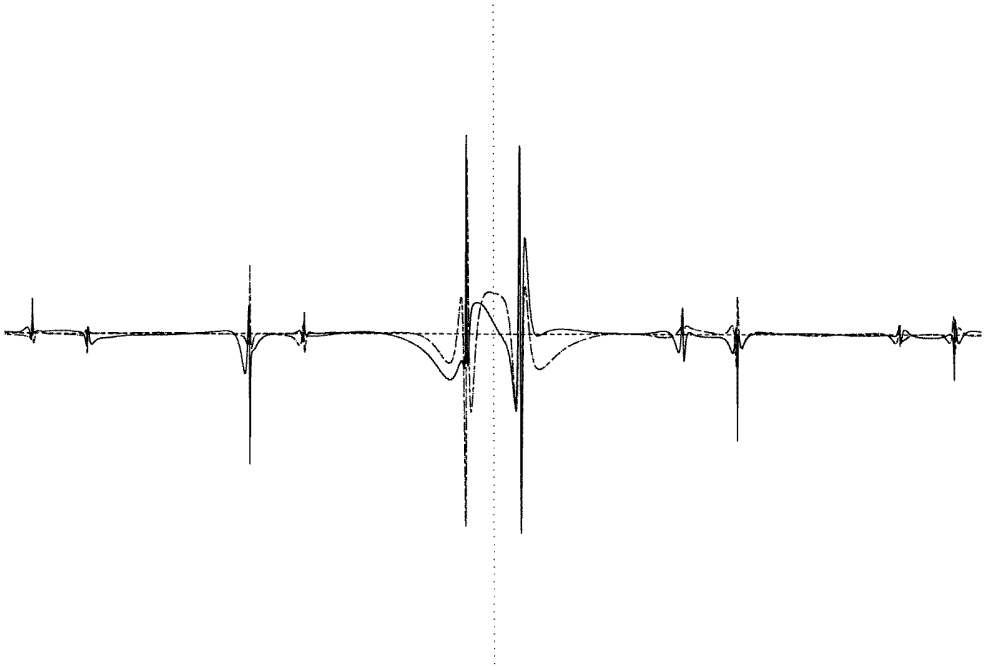

Figure 5. Wannier functions with p symmetry for GaAs in the (111) direction. ——: Ga; - - - -: As. The Ga function is centred at the atom to the left of the dotted mirror axis, and the As function at that to the right. The precise positions of the nuclei coincide with the most distinctive local maxima of the functions, which are due to the s-like parts present in all spheres.

The properties of the Wannier functions make them suitable for the explicit evaluation of various kinds of matrix element. Matrix elements of potentials that fall off sufficiently quickly, like those due to lattice imperfections, interfaces, or surfaces, can be calculated directly by performing an integration over a finite region in space, typically several unit cells. The matrix elements of the periodic operators can be evaluated in the original Bloch basis before the transformation into the Wannier basis is carried out.

As an example we consider the position operator. It can be split into a non-periodic part which is diagonal in the Wannier basis, and a periodic part $\boldsymbol{X}$ which is off-diagonal:

$$\langle \mu s' \boldsymbol{R}' | \boldsymbol{r} | \boldsymbol{R} \nu s \rangle = (\boldsymbol{R} + \boldsymbol{s}) \delta_{\boldsymbol{R}\boldsymbol{R}'} \delta_{ss'} \delta_{\nu\mu} + \langle \mu s' \boldsymbol{R}' | \boldsymbol{X} | \nu s \boldsymbol{R} \rangle. \tag{39}$$

The periodic part can be evaluated by means of the Bloch functions:

$$\langle \mu s' \boldsymbol{R}' | \boldsymbol{X} | \nu s \boldsymbol{R} \rangle = (1 - \delta_{\boldsymbol{R}\boldsymbol{R}'} \delta_{ss'} \delta_{\nu\mu}) \sum_{\boldsymbol{k} \in \mathcal{BZ}} \exp[-\mathrm{i}\boldsymbol{k} \cdot (\boldsymbol{R} - \boldsymbol{R}' + \boldsymbol{s} - \boldsymbol{s}')]$$
$$\times \sum_{nn'} \boldsymbol{e}(n', \boldsymbol{k})^{s'}_{\mu} \boldsymbol{e}(n, \boldsymbol{k})^{s\,*}_{\nu} \int_{WSC} \langle n'\boldsymbol{k} | \boldsymbol{r} \rangle \boldsymbol{r} \langle \boldsymbol{r} | n\boldsymbol{k} \rangle \, \mathrm{d}\boldsymbol{r}. \tag{40}$$

The integration is extended over only one Wigner–Seitz cell, so it can be performed without difficulty. The matrix elements are given in table 5. They are small compared to the cubic lattice constant of typically 10 au, and their decay is again due to the localized character of the Wannier functions.

Table 5. Values for dipole matrix elements for GaAs and AlAs in au. 1 indicates a Ga or Al Wannier function centred at $\boldsymbol{s}_1 = (111)\boldsymbol{a}/8$, and 2 an As Wannier function centred at $\boldsymbol{s}_2 = -(111)\boldsymbol{a}/8$.

	GaAs	AlAs
On site		
$\langle s\mathbf{1}\|z\|z\mathbf{1}\rangle$	0.034	−0.022
$\langle x\mathbf{1}\|z\|y\mathbf{1}\rangle$	0.008	−0.013
$\langle s\mathbf{2}\|z\|z\mathbf{2}\rangle$	0.034	−0.022
$\langle x\mathbf{2}\|z\|y\mathbf{2}\rangle$	0.009	−0.014
First neighbours		
$\langle s\mathbf{1}\|z\|s\mathbf{2}\rangle$	−0.024	0.003
$\langle s\mathbf{1}\|z\|x\mathbf{2}\rangle$	0.010	0.012
$\langle s\mathbf{1}\|z\|z\mathbf{2}\rangle$	0.040	0.032
$\langle x\mathbf{1}\|z\|s\mathbf{2}\rangle$	−0.006	−0.000
$\langle x\mathbf{1}\|z\|x\mathbf{2}\rangle$	0.002	−0.012
$\langle x\mathbf{1}\|z\|y\mathbf{2}\rangle$	0.012	−0.017
$\langle x\mathbf{1}\|z\|z\mathbf{2}\rangle$	0.006	−0.013
$\langle z\mathbf{1}\|z\|s\mathbf{2}\rangle$	0.051	−0.044
$\langle z\mathbf{1}\|z\|x\mathbf{2}\rangle$	−0.001	0.003
$\langle z\mathbf{1}\|z\|z\mathbf{2}\rangle$	−0.020	0.002

3.4. A homogeneous external electric field

We want to show how the Wannier functions can be used as a basis for the numerical solution when a homogeneous external electric field is applied. The eigenfunction with energy E is expanded in terms of layer Wannier functions (21) for layers perpendicular to the field direction:

$$|\boldsymbol{k}_\perp, E\rangle = \sum_{\nu l s} \Phi_{\nu s l}(E)|\boldsymbol{k}_\perp, \nu \boldsymbol{s} l\rangle. \tag{41}$$

$\Phi_{\nu s l}(E)$ is the envelope for the layer Wannier function with symmetry ν at basis atom s. Employing a scalar potential $\boldsymbol{F}\cdot\boldsymbol{r}$, the Schrödinger equation becomes

$$\sum_{\nu l s}\langle \boldsymbol{k}_\perp \mu \boldsymbol{s}' l'|\mathcal{H} + \boldsymbol{F}\cdot\boldsymbol{X}|\boldsymbol{k}_\perp \nu \boldsymbol{s} l\rangle \Phi_{\nu s l} = (E - \boldsymbol{F}\cdot(l\boldsymbol{a}_3 + \boldsymbol{s}'))\Phi_{\mu s' l'} \tag{42}$$

where the correction to the Slater–Koster parameters due to the periodic part of the dipole matrix elements is scaled by the field strength. If E is an eigenvalue and $L\boldsymbol{a}_3$ is the lattice period in the $\boldsymbol{a}_3$-direction, then $E + L\boldsymbol{F}\cdot\boldsymbol{a}_3$ is also an eigenvalue, and the corresponding envelope is

$$\Phi_{\nu, l+L, s}(E + L\boldsymbol{F}\cdot\boldsymbol{a}_3) = \Phi_{\nu l s}(E). \tag{43}$$

Thus, the solutions have to be determined for only one energy interval.

Let us consider an infinite superlattice. The Hamiltonian in the basis of the layer Wannier functions is an infinite band matrix, the width of which is determined by the number of neighbours taken into account. In order to obtain an approximation to the eigenvalues and eigenvectors of the infinite matrix, we consider a finite submatrix of dimension n. This is motivated by the expected localized character of the eigenvectors—which correspond to the Wannier–Stark resonances—due to the diagonal term in equation (42). We do not introduce periodic boundary conditions, so the finite matrix is still of band form. The band matrix can be transformed into a tridiagonal matrix by means of an algorithm (Givens rotations [16])

which maintains the band form in each step. Then selected eigenvalues can be calculated using the method of bisection. Focusing on eigenvalues with indices close to $n/2$, we find ones which are separated by $L\boldsymbol{F}\cdot\boldsymbol{a}_3$. The corresponding eigenvectors are found by inverse iteration. The dimension of the band matrix, i.e. the number of potential wells considered, depends on the desired numerical accuracy of the spacing $L\boldsymbol{F}\cdot\boldsymbol{a}_3$ between the eigenvalues.

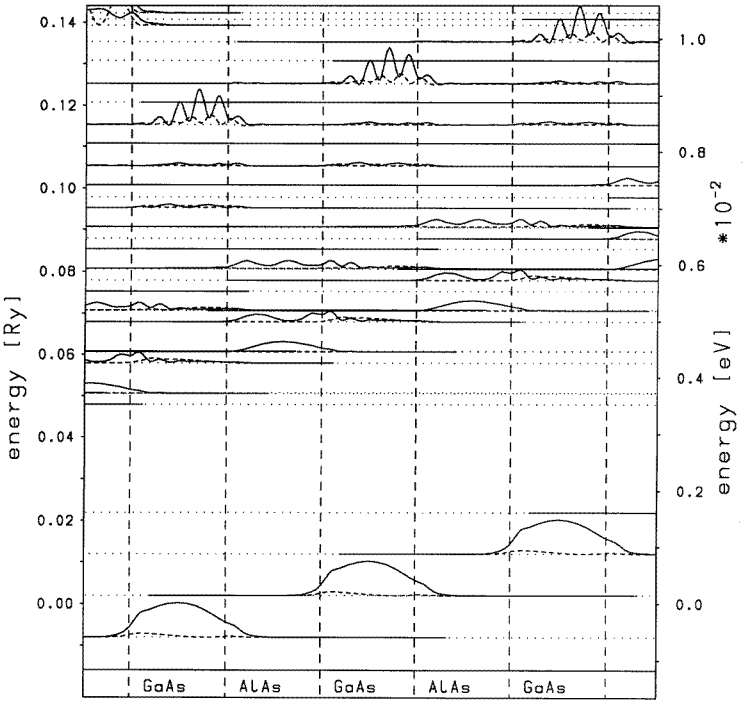

Figure 6. Squares of envelopes for a GaAs/AlAs superlattice with a (001) growth direction for $\boldsymbol{k} = 0$ and $\boldsymbol{F} = 50$ keV cm^{-1} in the growth direction. Only those states which show a considerable degree of localization are shown. ——: squares of envelopes $\Phi_s^2 + \Phi_z^2$ for Ga and Al. - - - -: squares of envelopes $\Phi_s^2 + \Phi_z^2$ for As. ·····: energy eigenvalues.

As an example, we considered a GaAs/AlAs superlattice with a (001) growth direction, which is also the field direction. The slabs consist of ten unit cells of GaAs and ten cells of AlAs, respectively, which are modelled by means of the respective bulk parameters. The results for the envelopes show many extended states with small amplitudes, and a few localized states with large amplitudes in one slab resulting from flat superlattice minibands (see figure 6). In particular the highest valence state is due to the valence band maximum (Γ_{15v}) of GaAs. The conduction band shows several states resulting from the X valley of AlAs. Above, there is a well localized state resulting from the conduction band minimum (Γ_{1c}) of GaAs. It can also be seen that the maximum of the envelopes is moved in opposite directions for the two basis atoms.

In contrast to an effective-mass approach, our method provides envelopes for each symmetry, and the wave function is known on a microscopic scale in terms of the envelopes and the Wannier functions.

In the example given above, we neglected the interface effects by simply using the bulk parameters for the different slabs. This was justified here because we only wanted to

demonstrate the usefulness of a localized basis in the treatment of an external field, which is clearly the dominating effect here.

In a precise calculation of the ground-state properties of layer structures, one has to calculate overlap and potential matrix elements connecting the bulk Wannier functions of the materials involved, which is a straightforward task once the Wannier functions are given explicitly. The determination of the eigenstates can then be performed using the sophisticated matching techniques recently developed by Hummel [17].

4. Conclusion

We have shown how generalized symmetry-adapted Wannier functions for diamond- and zinc-blende-type semiconductors can be constructed from Bloch functions. They form an orthogonal set, transform according to representations of the point subgroup, are differentiable, and are orthogonal to the core states. Two crucial points enter into the solution of the problem. The first is a precise Slater–Koster parametrization of the first-principles band structure. The second is the choice of the phase of the Bloch functions, for which a method could be established even in the case of the zinc-blende structure, which lacks inversion symmetry. Due to these properties, they can serve as a numerical basis equivalent to that of the Bloch functions with a precision that is only restricted by the number of bands included in the SK Hamiltonian.

Acknowledgment

Thanks are due to R Bader for his MAPW calculations.

Appendix. Treatment of degeneracies

In the case of a degeneracy at the point $\boldsymbol{k}$, there exists an arbitrariness in the first-principles eigenfunctions as well as in the eigenvectors of the model Hamiltonian belonging to the degenerate energy. This arbitrariness is connected to the fact that the representations under which either of them transform are determined only up to equivalence. We consider the little group of $\boldsymbol{k}$: $G(\boldsymbol{k}) = \{\{\beta, \boldsymbol{t}_\beta\}|\beta\boldsymbol{k} = \boldsymbol{k} + \boldsymbol{K}\}$. Here $\boldsymbol{t}_\beta$ denotes the non-primitive translation associated with the rotation β, and $\boldsymbol{K}$ a reciprocal-lattice vector. The degenerate Bloch functions transform in the following way:

$$\{\beta, \boldsymbol{t}_\beta\}|n\boldsymbol{k}\rangle = \sum_{n'} \widetilde{D}_{\boldsymbol{k}}(\beta)_{nn'}|n'\boldsymbol{k}\rangle \qquad \text{for } \beta \in G(\boldsymbol{k}) \tag{A1}$$

where the sum is extended over the degenerate states. The matrices $\widetilde{D}_{\boldsymbol{k}}(\beta)$ form an irreducible representation of $G(\boldsymbol{k})$, the dimension of which is the degree d of the degeneracy. The matrix elements of the representation are determined in the following way:

$$\widetilde{D}_{\boldsymbol{k}}(\beta)_{nn'} = \langle n'\boldsymbol{k}|\{\beta, \boldsymbol{t}_\beta\}|n\boldsymbol{k}\rangle. \tag{A2}$$

The integral can be reduced to the Wigner–Seitz cell, because $\beta\boldsymbol{k} = \boldsymbol{k}$.

Using (13) yields

$$\widetilde{D}_{\boldsymbol{k}}(\beta)_{nn'} = \sum_{\boldsymbol{R}\boldsymbol{R}'} \sum_{ss'} \exp[\mathrm{i}\boldsymbol{k}\cdot(\boldsymbol{s} - \boldsymbol{s}' + \boldsymbol{R} - \boldsymbol{R}')] \sum_{\nu\nu'} \widetilde{\boldsymbol{e}}(n, \boldsymbol{k})^{s'*}_{\nu'} \widetilde{\boldsymbol{e}}(n, \boldsymbol{k})^{s}_{\nu} \times \langle \nu'\boldsymbol{s}'\boldsymbol{R}'|\{\beta, \boldsymbol{t}_\beta\}|\nu\boldsymbol{s}\boldsymbol{R})\rangle. \tag{A3}$$

$\widetilde{e}(n,\boldsymbol{k})^s_\nu$ are the correct eigenvectors, still to be determined. From the transformation properties of the Wannier functions (16) and (A1), and $\beta\boldsymbol{k}=\boldsymbol{k}$, it follows that

$$\widetilde{D}_{\boldsymbol{k}}(\beta)_{nn'}=\exp\left[\mathrm{i}\boldsymbol{k}\cdot\boldsymbol{t}_{\beta^{-1}}\right]\sum_s\sum_{\mu\nu}\Gamma_s(\beta)^{-1}_{\nu\mu}\widetilde{e}(n,\boldsymbol{k})^{s\,*}_\mu\widetilde{e}(n',\boldsymbol{k})^s_\nu. \tag{A4}$$

In general, the representation defined by

$$D_{\boldsymbol{k}}(\beta)_{nn'}\equiv\sum_s\sum_{\mu\nu}\Gamma_s(\beta)^{-1}_{\nu\mu}\boldsymbol{e}(n,\boldsymbol{k})^{s\,*}_\mu\boldsymbol{e}(n',\boldsymbol{k})^s_\nu \tag{A5}$$

is a unitary representation of $G(\boldsymbol{k})$ equivalent to $D\sim k$. So there exists a unitary transformation U with

$$D_{\boldsymbol{k}}(\beta)=U\widetilde{D}_{\boldsymbol{k}}(\beta)U^{-1}\qquad\text{for all }\beta\in G(\boldsymbol{k}). \tag{A6}$$

The correct eigenvectors $\widetilde{e}(n,\boldsymbol{k})^s_\nu$ can be found by means of a projection operator technique:

$$\begin{aligned}\frac{d}{g}\sum_{\beta\in G(\boldsymbol{k})}\widetilde{D}_{\boldsymbol{k}}(\beta)_{nn}\sum_\mu\Gamma_s(\beta)^{-1}_{\nu\mu}\boldsymbol{e}(n,\boldsymbol{k})^{s\,*}_\mu&=\frac{d}{g}\sum_{\beta\in G(\boldsymbol{k})}\widetilde{D}_{\boldsymbol{k}}(\beta)_{nn}\sum_{n'}D_{\boldsymbol{k}}(\beta)_{nn'}\boldsymbol{e}(n',\boldsymbol{k})^{s\,*}_\nu\\&=\frac{d}{g}\sum_{\beta\in G(\boldsymbol{k})}\widetilde{D}_{\boldsymbol{k}}(\beta)_{nn}\sum_{n'pq}U_{np}\widetilde{D}_{\boldsymbol{k}}(\beta)_{pq}U^{-1}_{qn'}\boldsymbol{e}(n',\boldsymbol{k})^{s\,*}_\nu\\&=\sum_{n'pq}\delta_{np}\delta_{nq}U_{np}U^{-1}_{qn'}\boldsymbol{e}(n',\boldsymbol{k})^{s\,*}_\nu\\&=U_{nn}\sum_{n'}U^{-1}_{nn'}\boldsymbol{e}(n',\boldsymbol{k})^{s\,*}_\nu=U_{nn}\widetilde{e}(n,\boldsymbol{k})^{s\,*}_\nu.\end{aligned} \tag{A7}$$

g denotes the order of $G(\boldsymbol{k})$. The sums are extended over the degenerate band indices. In the third step we have used the orthogonality relations for irreducible representations of finite groups. Normalization yields the new eigenvectors $\widetilde{e}(n,\boldsymbol{k})^s_\nu$ up to a phase factor. The relative phase factors are determined by comparing the off-diagonal elements calculated according to (A5) with those from (A2).

In this way the freedom is removed which lies in the arbitrary orientation of the degenerate eigenfunctions, leading to the failure of the $\boldsymbol{k}\cdot\boldsymbol{p}$ procedure in the case of a degeneracy. Thus we obtain smooth functions in $\boldsymbol{k}$-space, and as a consequence well localized Wannier functions.

References

[1] Kohn W 1973 *Phys. Rev.* B **7** 4388
[2] Tejedor C and Vergés J A 1979 *Phys. Rev.* B **19** 2283
[3] Goodings D and Harris R 1969 *Phys. Rev.* **178** 1189
[4] Callaway J and Hughes A 1967 *Phys. Rev.* **156** 860
[5] Blount E 1962 *Solid State Physics* vol 13 (New York: Academic)
[6] Des Cloizeaux J 1964 *Phys. Rev.* **135** A685
[7] Bross H 1971 *Z. Phys.* **243** 311
[8] Teichler H 1971 *Phys. Status Solidi* b **43** 307
[9] Sporkmann B and Bross H 1994 *Phys. Rev.* B **49** 10 869
[10] Reser B I, Egorov R F and Shirikovskii V P 1968 *Phys. Status Solidi* b **26** 391
[11] Bader R 1994 MAPW calculations for semiconductors, unpublished
[12] Bross H and Bader R 1995 *Phys. Status Solidi* b **191** 369
[13] Gunnarsson O and Lundquist B 1976 *Phys. Rev.* B **13** 4274
[14] Papaconstantopoulos D A 1986 *Handbook of the Band Structure of Elemental Solids* (New York: Plenum)
[15] Vogl P, Hjalmarson H P and Dow J D 1981 *J. Phys. Chem. Solids* **44** 365
[16] Wilkinson J H 1965 *The Algebraic Eigenvalue Problem* (Oxford: Oxford University Press)
[17] Hummel W 1995 *PhD Thesis* Ludwig-Maximilians-Universität München